J Appl Electrochem (2014) 44:613–620
DOI 10.1007/s10800-014-0663-5

RESEARCH ARTICLE

Controlled electrodeposition of ZnO nanostructures for enhanced light scattering properties

Miriam M. Schwarz · Thilo Richter · Rion Pearson · Asman Tamang · Torsten Balster · Dietmar Knipp · Veit Wagner

Received: 16 September 2013 / Accepted: 6 January 2014 / Published online: 18 January 2014

Abstract This paper outlined how to control density and shape of electrodeposited ZnO nanorods to achieve high scattering properties. Light scattering at nanostructured metal–semiconductor interfaces is a proven method to improve absorption in photovoltaic devices. Adjustment of nanostructure shape and mean distance is critical to achieve efficient light scattering. A simple model is introduced that predicts maximal suppression of the specular transmitted light, resulting in maximal light scattering. This model predicts in an ideal case, 50 % nanostructure coverage of the electrode. Furthermore, an optimal nanostructure height has been determined depending on the incident wavelength and the refractive indices. Experimentally, the crystal density on ITO substrates was adjusted by pulsing the deposition potential, thus, removing the requirement for an additional seeding layer. The solution of the diffusion equation indicated a break-to-pulse ratio of at least 2.4 for an efficient control of the crystal density during pulsed electrodeposition. In addition, the structure height was set by varying the number of pulse cycles. Such tailored ZnO nanostructures showed a suppression of the specular transmitted light beam of 83.5 % and a diffusive forward scattering efficiency of 39 % at a wavelength of 406 nm. Thus, the optical absorption of e.g. an 80-nm thick polymeric active layer of P3HT could be increased by 47 % by applying such tailored ZnO nanostructures.

M. M. Schwarz · T. Richter · R. Pearson · A. Tamang · T. Balster · D. Knipp · V. Wagner (✉)
Research Center for Functional Materials and Nanomolecular Science, Jacobs University Bremen, Campus Ring 1, 28579 Bremen, Germany
e-mail: v.wagner@jacobs-university.de

Keywords Controlled electrodeposition of ZnO · Differently dense ZnO nanorods · Light scattering · Pulsed electrodeposition · Ion concentration profile

1 Introduction

Various nanostructure morphologies play an important role in the field of photovoltaics [1]. One-dimensional nanorods serve as a direct pathway for the charge carriers to the electrodes [2], nano-porous scaffolds are required for sufficient dye-loading in dye-sensitised solar cells [3], and various nanostructures are applied as anti-reflection coatings [4]. Generally, manifold morphological requirements have to be met depending on the application. Electrodeposition of ZnO is known to be an efficient method to achieve a wide range of nanostructured ZnO morphologies. The most prominent structure type of electrodeposited ZnO is nanorods [5]. However, 2D sheets [6] or many other morphologies [7, 8] are obtained by changing the deposition conditions.

Here, we focus on the design options of electrodeposited ZnO regarding properties for efficient light scattering. Light scattering in solar cells elongates the optical pathway of the incident light in the active layer. Thus, absorption and the overall device performance are increased. An enhanced absorption in organic solar cells is crucial, considering the trade-off between layer thickness and charge extraction [9]. An optimal layer thickness of 80 nm was found by Nam et al. [10] for a P3HT-based bulk heterojunction solar cell. Calculating the optical absorption of an 80-nm thick P3HT layer using Lambert's law shows that only 15 % of the energy of a 1.5 AM solar spectrum is absorbed within the layer [11, 12]. With increasing layer thickness, the optical absorption rises and saturates at

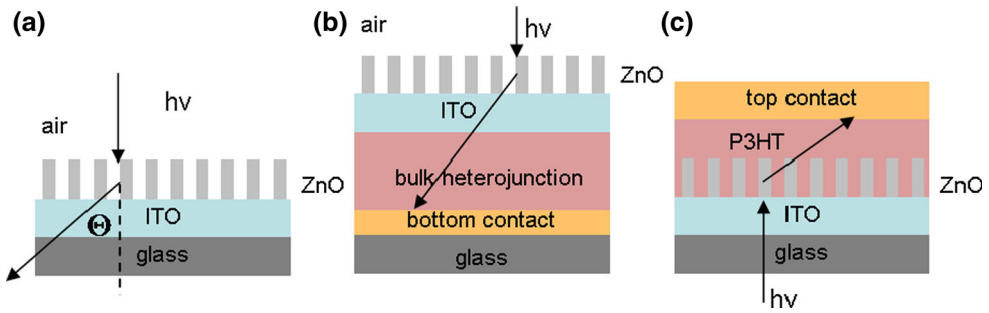

Scheme 1 **a** Test structure as used in the experiments: ZnO nanostructures on top of a glass/ITO substrate. **b** Cross-section of a bulk heterojunction solar cells with ZnO nanostructues on the ITO top contact for light scattering into the active layer of the bulk heterojunction solar cell. **c** Cross-section of a hybrid-organic solar cell with ZnO as *n*-type scaffold with light scattering properties

around 37 % for layers thicker than 1,000 nm, i.e. the absorption limit for infinitely thick layers is 37 %. This limit is caused by the band gap of P3HT which hinders absorption below 2.0 eV. Thick layers of 1,000 nm, however, are not ideal, since the extraction of generated charges becomes complicated in such thick layers of bulk heterojunctions [9]. Thus, innovative methods such as the application of nanostructured electrodes become very interesting (Scheme 1). It is known that the mean distances between such nanostructures, as well as their diameters and lengths, are very critical parameters for efficient light scattering [13, 14]. All in all, it is imperative to investigate and control the deposition of nanostructures in order to optimise their light scattering properties.

In the context of light scattering, zinc oxide is well suited as it is a wide bandgap semiconductor which does not absorb light in the visible region. Consequently, appropriate ZnO nanostructures will not absorb the light, but rather scatter it towards the active semiconducting layer of the solar cell. In addition, ZnO is known to be a promising window electrode material when doped [15]. Versatile ZnO nanostructures can be directly deposited onto the electrode material by electrodeposition. This deposition method does not only offer a wide range of morphological design options of the nanostructures [7, 16, 17]. It is also suitable for temperature sensitive substrates since it requires less then 100 °C for achieving deposition of high quality ZnO structures [18]. Electrodeposited ZnO nanostructures have been applied as Lambertian light scattering electrodes in polymeric solar cells [14]. It is also possible to electrodeposit ZnO periodically by applying a polymeric template [19]. In this report we show how to optimise the shape and density of electrodeposited ZnO nanorods for high light scattering properties at a particular wavelength. Firstly, we demonstrate that varying the deposition potential and applying it in pulses allows an adjustment of the crystal density. Furthermore, we solve the diffusion equation for a simplified system to determine an appropriate ratio between the pulses and the breaks which leads to an efficient increase in the crystal density. Secondly, we investigate the scattering properties of differently dense ZnO nanorod arrays. We observe a direct proportional relation between the suppression of the specular transmitted light intensity and the diffusively scattered light intensity and develop a model of how to maximise the suppression, thus maximising the scattered light intensity. The model suggests an ideal structure height depending on the wavelength of the incident light and the refractive indices of the material system. In accordance with these findings, we adjust the height of the ZnO structures for our system by choosing proper deposition times. Finally, we evaluate the scattering properties of the tailored structures for their application in organic P3HT solar cells and estimate an expected increase in absorption by 47 % due to scattering.

2 Experimental

ZnO was grown electrochemically from aqueous $Zn(NO_3)_2$ solution with potassium chloride (KCl) as a supporting electrolyte. A platinum (Pt) sheet was used as the counter electrode, an Ag/AgCl wire as the reference electrode and an indium tin oxide (ITO) covered glass slide as the working electrode. The following deposition parameters were chosen: electrolyte concentration $[Zn(NO_3)_2] = 5$ mM (0.037 g), support electrolyte concentration [KCl] = 100 mM (0.289 g), temperature of the solution $T = 75$ °C, applied voltage $V = -0.975$ V or $V = -0.775$ V versus Ag/AgCl (depending on the respective experiment).

To investigate the scattering properties of the electrodeposited ZnO nanostructures, the samples were illuminated with a laser of 406 nm wavelength. By rotating a photodetector in one degree steps around the sample, the scattered light at particular scattering angles between 90° and −90° is recorded. Between 10° and −10°, the step size was decreased to 0.25°.

3 Results and discussion

Applying a negative potential to the working electrode in an aqueous $Zn(NO_3)_2$ solution drives the reduction of NO_3^- which results in the production of OH^- ions close to the surface of the cathode [20]. The rising pH at the surface leads to the coverage of the electrode surface by a zinc hydroxide layer [18]. By a small thermal activation of less than 100 °C, ZnO nucleation occurs at energetically suitable nucleation sites of the surface. Figure 1a shows an AFM image of the blank ITO substrate and for comparison, Fig. 1b shows a SEM image of ZnO nanostructures electrodeposited at constant potential of −0.975 V for 300 s. Very few ZnO crystals can be observed on top of the ITO surface with a mean spacing of several hundred nanometers up to a micrometer. We assume that the rather sparse formation of ZnO crystals on ITO is due to depletion of the electrolyte around the ZnO nuclei. During crystal growth,

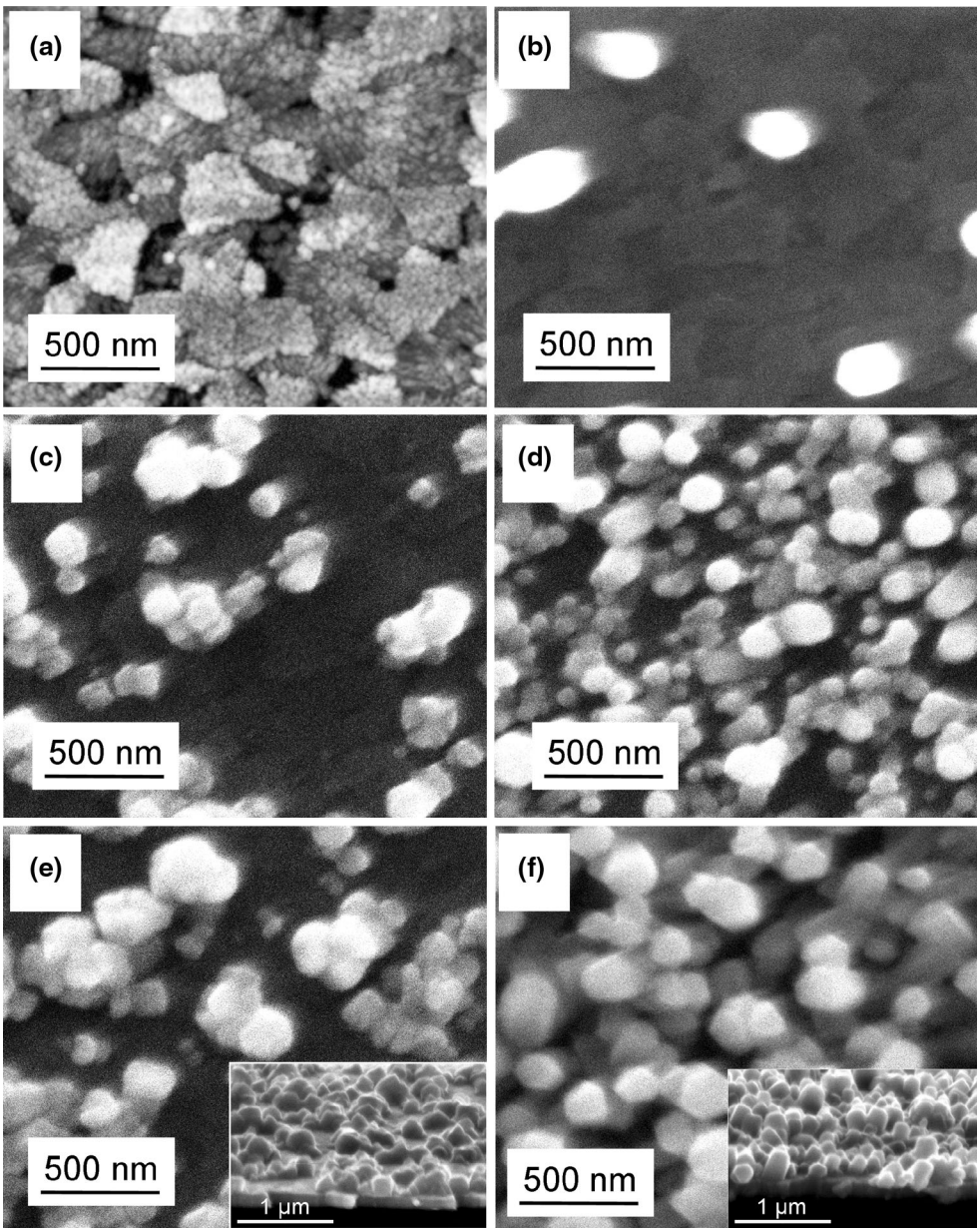

Fig. 1 **a** AFM image of a blank glass/ITO substrate (*grey scale* corresponds to 16 nm), **b–f** SEM images of ZnO crystals electrodeposited on glass/ITO under constant deposition voltage of −0.975 V for 300 s (**b**), under pulsed deposition voltage of −0.775 V with 30 × 10 s pulses (**c**), under pulsed deposition voltage of −0.975 V with 30 × 10 s pulses (**d**), under pulsed deposition voltage of −0.775 V with 60 × 10 s pulses (**e**, *inset* side view), under pulsed deposition voltage of −0.975 V with 60 × 10 s pulses (**f**, *inset* side view)

the ZnO nuclei consume ions from the electrolyte, which causes a depletion region of a certain radius around the nuclei. Within this depletion region, the electrolyte concentration is not sufficient for the formation of further nuclei at energetically less favourable sites. To increase the crystal density, we control the electrolyte concentration at the surface by pulsing the applied potential. By switching off the potential after a short deposition time, the NO_3^- reduction stops, no further OH^- ions are produced and the ZnO growth abates. The depletion radii around the nuclei dissolve and the electrolyte concentration at the surface relaxes to the concentration of the bulk solution. By applying a second potential pulse, the ZnO production starts over again and energetically less favourable nucleation sites can be occupied, since the concentration of the electrolyte at the surface is relaxed to the high bulk value. Already existing nuclei continue growing. Thus, controlling the electrolyte concentration at the surface of the working electrode by a pulsed deposition potential allows the occupation of a broader energetic distribution of nucleation sites. This boosts the overall amount of nuclei and finally the ZnO crystal density.

To estimate an appropriate pulse to break ratio of the applied potential, the one-dimensional diffusion equation of the system is solved.

$$\frac{\partial C(x,t)}{\partial t} = D \cdot \frac{\partial^2 C(x,t)}{\partial x^2} \tag{1}$$

The idealised system assumes an infinite planar electrode area with a homogeneous growth mode. Here, x is the vertical distance from the electrode, with the electrode positioned at $x = 0$. D is the diffusion constant of the relevant ion species with concentration C(x,t) and t is the time. The initial concentration distribution before a potential is applied is given by the bulk concentration C_0. Assuming that every NO_3^- approaching the surface is instantly reduced, the nitrate concentration is set to zero at $x = 0$.

$$C(x, t = 0) = C_0 \tag{2}$$

$$C(x = 0, t) = 0 \quad \text{for } t > 0 \tag{3}$$

The analytical solution of the one-dimensional diffusion equation for these initial and boundary conditions can be obtained by using the Laplace transformation technique carried out with respect to t which leaves the dependence of C on x unchanged.

$$D \cdot \frac{\partial^2 \overline{C}(x,s)}{\partial x^2} - s \cdot \overline{C}(x,s) + C_0 = 0 \tag{4}$$

The concentration profile becomes

$$\bar{C}(x,s) = C_0 \left(\frac{1}{s} - \frac{1}{s} \exp\left(-\sqrt{\frac{s}{d}} x \right) \right) \tag{5}$$

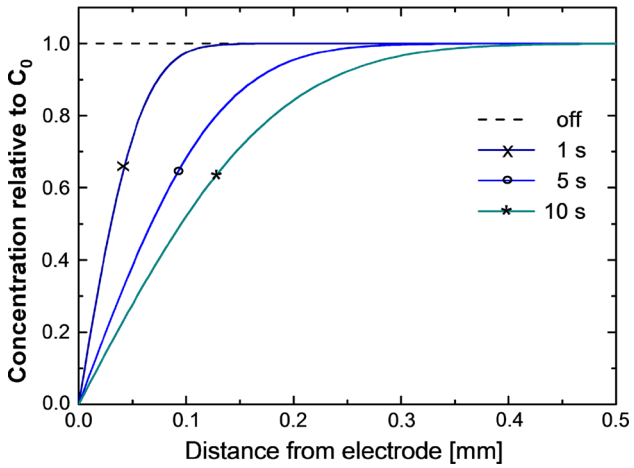

Fig. 2 Concentration profile of an aqueous 5 mM $Zn(NO_3)_2$ solution as function of distance from the electrode and duration of deposition assuming $D_{\text{nitrate}} = 1.902 \times 10^{-5}$ cm^2 s^{-1}

and can finally be determined as function of time by carrying out the inverse Laplace transformation which yields:

$$C(x,t) = C_0 erf\left(\frac{x}{2\sqrt{Dt}} \right) \tag{6}$$

Figure 2 shows the development of the NO_3^- concentration within the first 10 s of applying a potential with $D_{\text{nitrate}} = 1.902 \times 10^{-5}$ cm^2 s^{-1} [21]. The concentration gradient becomes shallower with increasing time.

These concentration profiles at certain pulse durations $t = t_{\text{pulse}}$ given by Eq. 6 can now be used as initial conditions for solving the diffusion equation after switching the potential off. The boundary condition is now conservation of number of ions at the sample surface and is given by.

$$\left. \frac{dC(x,t_r)}{dx} \right|_{x=0} = 0 \tag{7}$$

Figure 3 shows a surface plot of the numeric solution of the one-dimensional diffusion equation with the given boundary conditions after the Laplace transformation for $C_0 = 5$ mmol. It can be observed that the concentration of the nitrate ions rises immediately after the voltage is switched to 0 V. This rise is initially fast and then slows down gradually. In order to define an appropriate on/off ratio of the pulsed deposition potential, we define a relaxation time t_{relax} at which the nitrate concentration at the electrode has reached 63 % (1 − 1/e) of the bulk concentration after switching of the deposition potential.

$$t_{\text{relax}} \text{ at } C = \left(1 - \frac{1}{e}\right) C_0 \tag{8}$$

Pulse durations from 1 to 30 s were examined and a linear relation between pulse and break duration is obtained

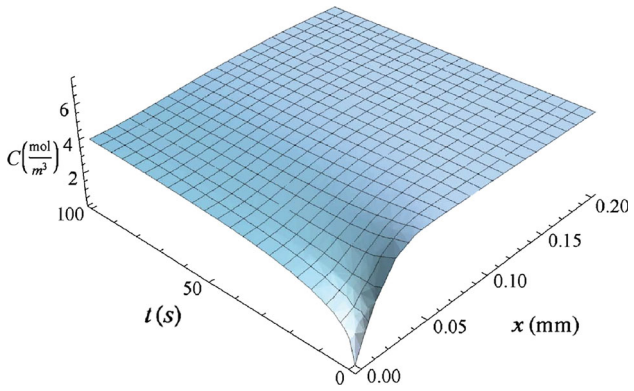

Fig. 3 Relaxation of the concentration profile after an initial 10 s pulse given by numerical solution of the diffusion equation for $D_{\text{nitrate}} = 1.902 \times 10^{-5}$ cm^2 s^{-1} and $C_0 = 5$ mM

with a slope of 2.4. It follows that the pause between pulses should be chosen at least 2.4 times as long as the duration of each pulse to reach a relaxation of the concentration to 63 % or beyond.

To prove the pulsing model, we deposited ZnO under the same deposition conditions and duration as in Fig. 1b, but now with voltage pulses of 30 times 10 s and 20 s voltage breaks between each pulse ensuring at least 50 % concentration relaxation. As shown in Fig. 1d, the crystal density increased significantly. As expected, a height distribution of the rods can be observed. With lower deposition voltages of −0.775 V using 30 × 10 s voltage pulses a reduced structure density is achieved (Fig. 1c) compared to higher deposition voltages (Fig. 1d). Due to lower driving voltage less nucleation sites are accessible in this case.

This type of ZnO nanostructures deposited on ITO can be used as a test system (Scheme 1a) for a possible application in photovoltaic devices, e.g. in bulk heterojunction solar cells, where ZnO nanostructures are deposited on top of the window electrode to scatter the light towards the active layer of the device (see Scheme 1b), or in hybrid-organic solar cells where ZnO is used as a n-type scaffold with light scattering properties (Scheme 1c).

To investigate the interdependence of structure density and light scattering properties, angle-resolved diffusive transmission spectra of all samples were recorded (Fig. 4). The specular transmitted light beam at zero degrees is reduced, i.e. partly suppressed for all samples. The samples with the lowest and medium structure densities show the same suppression of the transmitted light intensity of 33 % (Fig. 4; Table 1, sample b and c). The sample with the highest structure density features a much higher suppression of 48 % (Fig. 4a; Table 1, sample d). Since ZnO is a wide bandgap semiconductor with a bandgap in the range of 3.2–3.4 eV [22], we exclude absorption at 406 nm (3.05 eV). Thus, the reason for suppression of the transmitted light intensity has to be scattering. Indeed, a considerable amount of scattered light intensity is observed between scattering angles of −90° and 90° with respect to the specular transmitted light beam at zero degree. Integration of the solid angle intensities over all angles shows that the total scattering intensity for the samples of lowest and medium density is 19.6 and 20.6 %, respectively (see Table 1) and thus almost the same. This is in accordance with the observation of the suppression of the specular transmitted light intensity for these two samples. The sample with structures of medium density however features a scattering maximum towards higher scattering angles (Fig. 4, sample c), which is more appropriate for photovoltaic applications. The sample of highest structure density shows the highest total scatter intensity of 26.1 % (Fig. 4, sample d). This was also expected due to the highest suppression of the specular transmitted light intensity.

Thus, a clear relation between the suppression of the specular transmitted light intensity and the scattering intensity is observed. According to this trend, higher suppression of the specular transmitted light intensity will lead to higher scattering intensities. In the following, we consider a further adjustment of the ZnO structures to achieve higher suppression and, hence, optimised scattering properties.

For this purpose, we follow the approach of Battaglia et al. [23] and restrict the analysis to 0°, i.e. the specular transmitted light beam. When light reaches the interface of the ZnO rods and air, the relative phase of the light changes according to the refractive index of the respective materials (Scheme 2). The resulting phase shift between the waves propagating through ZnO and air can be expressed by Eq. 9. The intensity of the transmitted light beam depends on this phase shift and on the fraction of occupied area p of the ZnO nanorods (p_{ZnO}) and the surrounding air (p_{air}) (Eq. 10).

$$\Delta\phi = 2\pi(n_{\text{ZnO}} - n_{\text{air}}) \cdot \frac{h}{\lambda_0} \tag{9}$$

$$\begin{aligned} I_{\text{transmitted}} &\propto \left| p_{\text{ZnO}} + p_{\text{air}} \cdot e^{i\Delta\phi} \right|^2 \\ &= 1 - 4p_{\text{ZnO}}(1 - p_{\text{ZnO}}) \cdot \sin^2\left(\pi(n_{\text{ZnO}} - n_{\text{air}})\frac{h}{\lambda_0}\right) \end{aligned} \tag{10}$$

Figure 5a shows the theoretical intensity of the specular transmitted light intensity in dependence of the average rod height for different ZnO occupancy fractions according to Eq. 10. It can be seen that the intensity of the transmitted light is minimised for a ZnO coverage of 50 % ($p_{\text{ZnO}} = 0.5$). Furthermore, the intensity of the transmitted light beam depends on the height of the ZnO rods. For high suppression of the specular transmitted light intensity, the ratio between the ZnO rod height and the wavelength

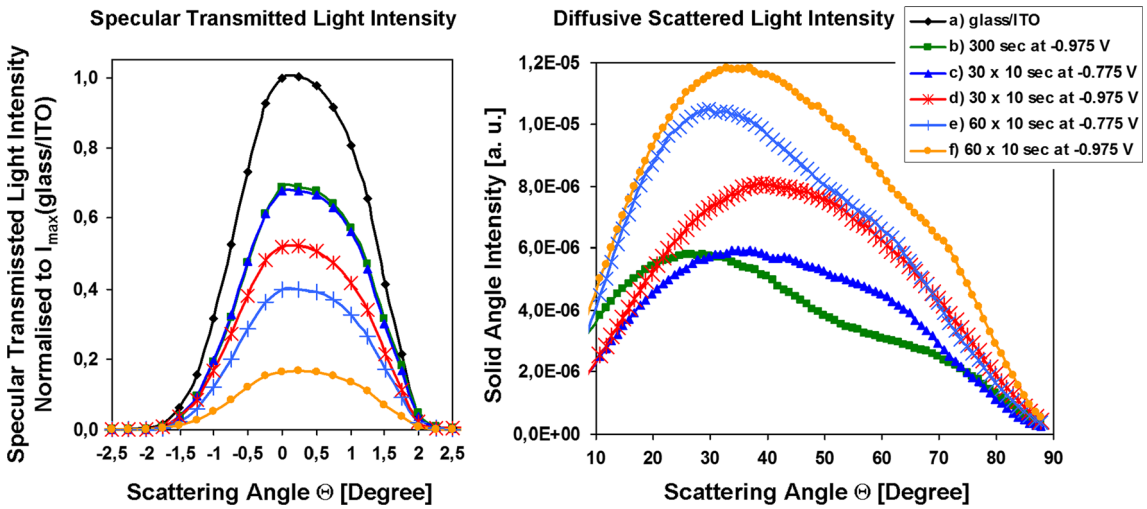

Fig. 4 Angle-resolved diffusive transmission spectra at 406 nm wavelength of *a* blank glass/ITO substrate, *b* ZnO crystals electrodeposited on glass/ITO under constant deposition voltage of −0.975 V for 300 s, *c* under pulsed deposition voltage of −0.775 V with 30 × 10 s pulses, *d* under pulsed deposition voltage of −0.975 V with 30 × 10 s pulses, *e* under pulsed deposition voltage of −0.775 V with 60 × 10 s pulses, *f* under pulsed deposition voltage of −0.975 V with 60 × 10 s pulses

Table 1 Experimentally determined rod height, fraction of area occupied by ZnO, specular light intensity (normalised to maximal light intensity of glass/ITO sample) and scattered light intensity in % for differently deposited samples

	a Glass/ITO	b 300 s at −0.975 V	c 30 × 10 s at −0.775 V	d 30 × 10 s at −0.975 V	e 60 × 10 s at −0.775 V	f 60 × 10 s at −0.975 V
Rod height (nm)	0	260	85	85	170	170
Fraction of area occupied by ZnO	0	0.07 ± 0.02	0.18 ± 0.04	0.40 ± 0.05	0.19 ± 0.04	0.33 ± 0.05
Specular light intensity in %	1	68.7	67.8	51.9	39.9	16.5
Scattered light intensity in %	–	19.6	20.6	26.1	32.5	39.0

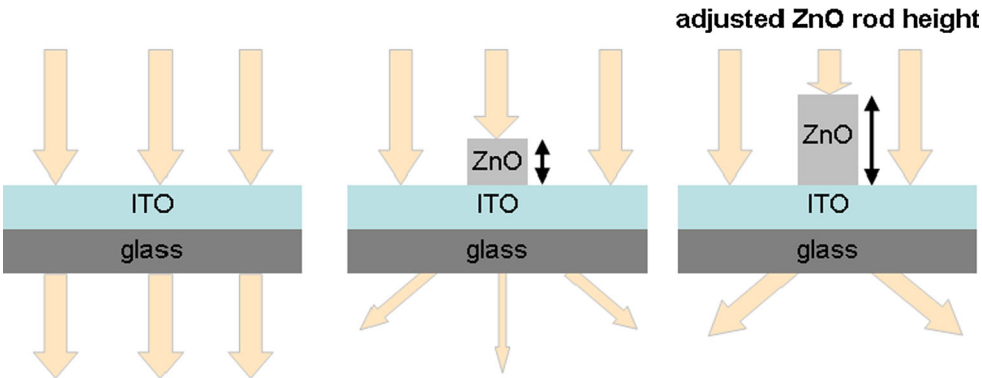

Scheme 2 Incident light propagating through ZnO and air. Without ZnO nanorods, the incident light is transmitted without scattering. With ZnO nanostructures, parts of the incident light is transmitted and parts are scattered. For an adjusted rod height, all of the incident light is scattered and the specular transmitted light intensity is suppressed to zero

should be chosen such that the propagating waves of each material interfere destructively when transmitted. This is the case for a phase shift of 180°. Thus, optimal heights can be obtained by $h = \lambda_0/(2\Delta n)$. In our experiments, utilising a wavelength of 406 nm, the optimal ZnO height is about 170 nm for $n_{air} = 1$ and $n_{ZnO} = 2.2$ [24].

According to these considerations, we have adjusted the average height of the ZnO rods by doubling the amount of pulses and, thus, increasing the deposition time. Figure 1e and f show SEM images of the resulting structures. For both deposition voltages, the doubled amount of pulses results clearly in bigger structures. In the side view, (insert in

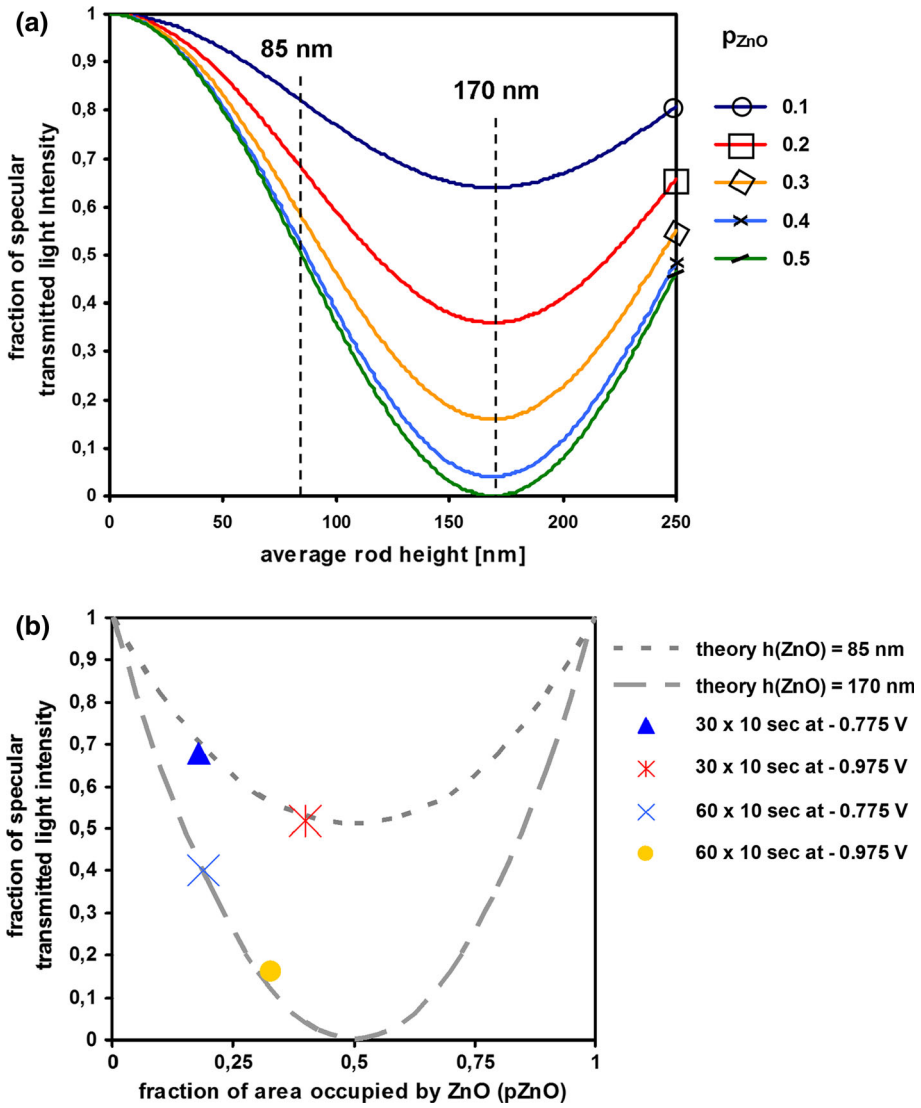

Fig. 5 **a** Theoretical interdependence between the specular transmitted light intensity and the average rod height for different fractions of area occupied by ZnO, **b** theoretical interdependence between the specular transmitted light intensity and the fraction of area occupied by ZnO for 85 and 170 nm rod heights including experimental data points

Fig. 1e, f), it can be seen that the coverage of crystals with an approximate height of 170 nm is around 50 %. As expected, this optimised crystal structure takes significant influence on the suppression of the specular transmitted light intensity (Fig. 4, sample e and f). Crystals of an average height of 170 nm cause a much higher suppression of the incident beam intensity. At a deposition voltage of −0.775 V the suppression of the specular transmitted light intensity increases from 32.2 to 60.1 % and structures deposited at −0.975 V show an increase from 48.1 to 83.5 % with doubled deposition time. This effect is also reflected in the respective angle-resolved diffusive transmission spectra shown in Fig. 4. For samples deposited at −0.775 V, a significant increase at lower angles around 30° and a slight increase for higher angles around 60° can be observed (Fig. 4, sample e). The total intensity of scattered light increases with longer deposition times from 20.6 % to 32.5 %. For deposition voltage of −0.975 V, the scattered light is broadly distributed over all angles and the structures show good scattering properties even at angles >70° (Fig. 4, sample f). The total intensity of scattered light increases with doubled deposition times from 26.1 to 39.0 %. In Fig. 5b, the experimental findings are compared to the theoretical values obtained from Eq. 10. The experimental values extracted from the SEM images for pulsed samples (summarised in Table 1) are in good agreement with the theory.

The mean scattering angle of the sample with best scattering properties can be calculated to 56.6°. Within a 80 nm thick P3HT layer, this angle relates to an optical pathway of 145 nm which will result in an 47 % increase of the optical absorption from 14.6 to 21.4 % for direct transmission (excluding reflection of the light at the metal back contact, which will further enhance absorption). Thus, an improvement towards the limit of an infinite layer is achieved. Considering Snell's law the effective angle within the P3HT layer is slightly reduced.

To achieve similar results in case of the application of ZnO structures as a scaffold in hybrid-organic solar cells, where e.g. P3HT is infiltrated as p-type semiconductor (see Scheme 1c), the averaged height of the ZnO nanostructures requires an adjustment according to the refractive index of the infiltrated organic material which then replaces air. For P3HT, an optimal ZnO rod height can be calculated to be approximately 250 nm with a refractive index of the anisotropic P3HT material of $n_{P3HT} = 1.4$ at 406 nm [12]. In our experiments, this could be simply achieved by longer deposition times. Further optimisation can be obtained by taking surface reflections and layer interference effects into account.

4 Conclusion

By means of a simple model, we have shown how the height and density of nanostructures can be refined to optimise scattering properties. The optimal structure height depends on the wavelength of the incident light and the refractive indices of the materials. For a ZnO/air system and an incident wavelength of 406 nm, 50 % of the electrode needs to be covered by ZnO nanostructures. Furthermore, the ideal height of the ZnO nanostructures is 170 nm. We have demonstrated that the structure density of electrochemically deposited ZnO crystals can be controlled by pulsing the deposition potential. Here, the ideal break-to-pulse ratio is 2.4 or more. Furthermore, we have shown that the crystal height can be adjusted by varying the number of pulse cycles. Such an electrochemically tailored ZnO nanostructure array features a high scattering efficiency of 39 % with a mean scattering angle of 56.6°. At this scatter angle, the optical pathway is increased from e.g. 80 nm to 145 nm. This leads to an increase in the optical absorption by 47 % in case of a P3HT layer corresponding to 58 % of the absorption limit of an infinitely thick layer.

References

1. Macaira J, Andrade L, Mendes A (2013) Reviw on nanostructured photoelectrodes for next generation dye-sensitized solar cells. Renew Sustain Energy Rev 27:334–349
2. Chen JY, Hsu FC, Sung YM, Chen YF (2012) Enhanced charge transport in hybrid polymer/ZnO-nanorod solar cells assisted by conductive small molecules. J Mater Chem 22:15726
3. Sakai N, Miyasaka T, Murakami TN (2013) Efficiency enhancement of ZnO-based dye-sensitized solar cells by low-temperature TiCl4 treatment and dye optimization. J Phys Chem C 117:10949–10956
4. Yu R, Lin Q, Leung SF, Fan Z (2012) Nanomaterials and nanostructures for efficient light absorption and photovoltaics. Nano Energy 1:57–72
5. Peulon S, Lincot D (1996) Cathodic electrodeposition from aqueous solution of dense or open-structured zinc oxide films. Adv Mater 8:166–169
6. Illy BN, Ingham B, Ryan MP (2010) Effect of supersaturation on the growth of zinc oxide nanostructured films by electrochemical deposition. Cryst Growth Des 10:1189–1193
7. Xu F, Lu Y, Xie Y, Liu Y (2009) Controllable morphology evolution of electrodeposited ZnO nano/micro-scale structure in aqueous solution. Mater Des 30:1704–1711
8. Yoshida T, Tochimoto M, Schlettwein D, Wöhrle D, Sugiura T, Minoura H (1999) Self-Assembly of ZnO thinfilms modified with tetrasulfonated metallophtalocyanines by one-step electrodeposition. Chem Mater 11:2657–2667
9. Deibel C, Dyakonov V (2010) Polymer–fullerene bulk heterojunction solar cells. Rep Prog Phys 73:096401
10. Nam YM, Huh J, Jo WH (2010) Optimization of thickness and morphology of active layer for high performance of bulk-heterojunction organic solar cells. Sol Energy Mater Sol Cells 94:1118–1124
11. Hecht (2003) Optics, 4th edn. Addison-Wesley Longman, Amsterdam
12. Pittner S, Lehmann D, Zahn DRT, Wagner V (2013) Charge transport analysis of poly(3-hexylthiophene) by electroreflectance spectroscopy. Phys Rev B 87:115211
13. Brönstrup G, Jahr N, Leiterer C, Csaki A, Fritzsche W, Christiansen S (2010) Optical properties of individual silicon nanowires for photonic devices. ACS Nano 4:7113–7122
14. Tena-Zaera R, Elias J, Levy-Clement C (2008) ZnO nanowire arrays: optical scattering and sensitization to solar light. Appl Phys Lett 93:233119
15. Noriega R, Rivnay J, Goris L, Kälblein D, Klauk H, Kern K, Thompson LM, Palke AC, Stebbins JF, Jokisaari JR, Kusinski G, Salleo A (2010) Probing the electrical properties of highly-doped Al:ZnO nanowire ensembles. J Appl Phys 107:074312
16. Illy BN, Cruickshank AC, Schumann S, Da Campo R, Jones TS, Heutz S, McLachlan MA, McComb DW, Riley DJ, Ryan M (2011) Electrodeposition of ZnO layers for photovoltaic applications: controlling film thickness and orientation. J Mater Chem 21:12949–12957
17. Prasad BE, Kamath PV, Ranganath S (2012) Electrodeposition of ZnO coatings from aqueous $Zn(NO_3)_2$ baths: effect of Zn concentration, deposition temperature, and time on orientation. J Solid State Electrochem 16:3715–3722
18. Goux A, Pauporte T, Chivot J, Lincot D (2005) Temperature effects on ZnO electrodeposition. Electrochim Acta 50:2239–2248
19. Oh S, Nagata T, Volk J, Wakayama (2012) Nanoimprint for fabrication of highly ordered epitaxial ZnO nanorods on transparent conductive oxide films. Appl Phys Express 5:095003
20. Izaki M, Omi T (1996) Transparent zinc oxide films prepared by electrochemical reaction. Appl Phys Lett 68:2439–2440
21. Linde DR (2003) Handbook of Physics and Chemistry. CRC Press, Boca Raton
22. Inguanta R, Garlisi C, Spano T, Piazza S, Sunseri C (2013) Growth and photoelectrochemical behaviour of electrodeposited ZnO thin films for solar cells. J Appl Electrochem 43:199–208
23. Battaglia C, Boccard M, Haug FJ, Ballif C (2012) Light trapping in solar cells: when does a Lambertian scatterer scatter Lambertianly? J Appl Phys 112:094504
24. Jellison GE Jr, Boatner LA (1998) Optical functions of uniaxial ZnO determined by generalized ellipsometry. Phys Rev B 58:3586–3589